Some observations on polarized neutron reflectivity in applied fields

2008 J. Phys.: Condens. Matter 20 295216

(http://iopscience.iop.org/0953-8984/20/29/295216)

J. Phys.: Condens. Matter **20** (2008) 295216 (11pp) doi:10.1088/0953-8984/20/29/295216

Some observations on polarized neutron reflectivity in applied fields

A R Wildes[1], M Björck[2,3] and G Andersson[2]

[1] Institut Laue Langevin, BP 156, 38042 Grenoble Cedex 9, France
[2] Department of Physics and Materials Science, Box 530, Uppsala University, SE-751 21 Uppsala, Sweden
[3] Paul-Scherrer Institute, CH-5200 Villigen PSI, Switzerland

E-mail: wildes@ill.fr

Received 28 March 2008, in final form 4 June 2008
Published 1 July 2008
Online at stacks.iop.org/JPhysCM/20/295216

Abstract
Unpolarized neutron reflectivity measurements on FeCo/Pt and Fe/Co superlattices have revealed a number of interesting features when a relatively large field was applied normal to the samples' surface. Some of the features, which include oscillations and Yoneda scattering below the critical edge, can be understood by calculating the polarization-dependent reflectivities and transmissions of the samples. Measurements with polarization analysis, however, show that the Zeeman-split reflected beams, expected in reflectivity experiments in an applied magnetic field, do not appear to have a unique spin state. The interpretation of the data is believed to lie in a non-collinearity between the axis for the reflected neutron beam polarization and the axis for the polarization analysis.

1. Introduction

Neutron reflectivity is often used to characterize the structure and properties of magnetic thin films, multilayers and superlattices. Most of the studies have focussed on the measurement of the magnetic structure as a function of depth in the sample. Neutron scattering at grazing incidence is also sensitive to in-plane structures, and there is increasing interest in using the technique to probe in-plane magnetic properties, including domain structures and patterned samples [1]. The development of neutron reflectivity techniques is relatively recent and ongoing, and the measurements sometimes show surprising results. This paper reports on the observation of some remarkable features in a neutron reflectivity experiment when applying a substantial magnetic field to the sample, and the implications of the observations on the theory of polarized neutron reflectometry.

The interaction of the neutron magnetic moment, $\boldsymbol{\mu}_n$, with the magnetic induction, $\mathbf{B}$, is determined by the potential

$$\hat{V}_m = -\boldsymbol{\mu}_n \cdot \mathbf{B}, \tag{1}$$

which is of a similar size to the nuclear potential. When applied to unpaired electrons in a sample, it is well known that the neutron cross-section, which includes reflectivity, is given from the components of the magnetization in the sample that are perpendicular to the scattering vector, $\mathbf{Q}$ [2, 3]. The technique is an extremely sensitive probe for measuring the magnetization density as a function of depth, especially when combined with neutron polarization analysis.

The neutron spin may be flipped on scattering from a sample magnetization that is perpendicular to both $\mathbf{Q}$ and the spin axis. In an applied field of strength H, the neutron has a Zeeman potential energy relative to the field equal to $\pm\mu_n \cdot \mu_0 H$. The kinetic energy of the neutron is proportional to the square of its de Broglie wavenumber k. On spin flip scattering, this will change by twice the Zeeman energy. The total energy of the neutron remains unchanged. The kinetic energy change is very small, $\sim$0.1 μeV T^{-1}, which is normally much smaller than the resolution of a neutron scattering experiment and hence is ignored.

In reflectivity, however, the important components of the wavevectors are normal to the sample. The energies associated with these components are of the same order as the Zeeman energy. The kinetic energy change results in a splitting of the reflected beam which is easily measured in an applied field [4]. The scattering diagram for a reflectivity experiment is shown in figure 1. In reciprocal space, reflection is represented by a 'surface streak' normal to the sample surface. The incident beam makes an angle of θ_i with the surface. Specular reflection is often defined such that the angle of the reflected beam equals the angle of the incident beam, $\theta_f = \theta_i$. If the

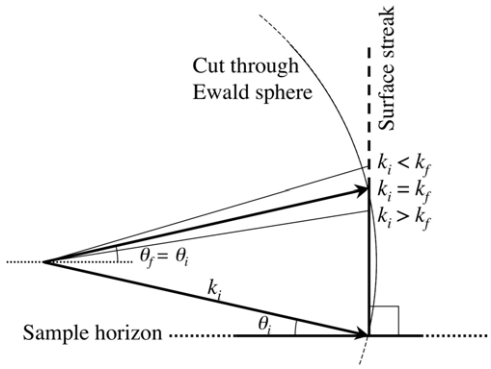

Figure 1. Schematic representation for neutron reflectivity in the presence of an external field. The incident beam, with wavenumber k_i, makes an angle of θ_i with the sample surface and the final beam, k_f, makes an angle θ_f. If the neutron undergoes spin flip with respect to the field, $k_f \neq k_i$.

neutron undergoes a kinetic energy change, however, the final wavenumber, k_f, will not equal the initial, k_i. Following from an Ewald construction, the momentum triangle must still close on the surface streak to see any scattering. Hence, the final angle will follow the equation [4]:

$$\theta_f^2 \approx \theta_i^2 \pm 1.47 \times 10^{-6} \mu_0 H \cdot \lambda^2, \qquad (2)$$

where $\mu_0 H$ is measured in Tesla and the wavelength, λ, is given in Ångströms. To avoid confusion, specular scattering will hereafter be defined such that **Q** is parallel to the surface normal.

In the initial experiment that observed this effect [4], a field was applied normal to a cobalt film in an attempt to magnetically saturate the sample along **Q**. The neutron is only sensitive to the components of the magnetization that are perpendicular to **Q**, hence it was hoped that the reflectivity would only be due to nuclear contrast. The field was insufficient, and a splitting in the reflected beams was observed [4]. More recently, the same trick was applied to Fe/Co and FeCo/Pt superlattices to characterize the structural properties of these materials, which had been investigated in previous studies using other techniques [5–8]. The experiments succeeded when fields of 3 T were applied normal to the sample, and the data could be fitted without considering magnetization [9].

Some measurements made in smaller applied fields, however, showed unusual features in the scattering that warranted further investigation. These observations form the subject of this paper, and their explanation reveals some interesting points on the interpretation and theory of polarized neutron reflectivity.

The derivation of a complete description of grazing incidence neutron scattering is demanding, both in terms of parameterizing a usable structure for the modelling, and of the theory. Such modelling can be highly labour intensive, and can obscure the source of certain features. On the other hand, as will be shown in this paper, a qualitative explanation for some of the features can be quickly derived from a far simpler treatment. Further measurements with polarization analysis have raised the issue of possible discrepancies between the neutron polarization axis and the instrument analysis axis. These issues have been addressed for measurements in zero field, however the application of a magnetic field may need to be considered in the future development of the theory.

It should be stressed that, while the effects reported in this paper are generic to polarized neutron reflectivity, they are probably enhanced by the structures of the samples studied. Full details of these specific structures are reported elsewhere [9], however simple approximations to the structures suffice to explain the features. As the subject of the paper is more a comment on the technique than a comment on the samples, the detailed structures will not be given outside the approximations.

2. Experiments

Measurements of two samples are presented in this paper. Both samples were grown by sputter deposition on substrates of (001) MgO. Listing the layers from the substrate:

- $MgO/Fe_{5.7\ Å}/Pt_{39Å}/[\{Fe_{0.36}Co_{0.64}\}_{25Å}/Pt_{35Å}]_{40}$ (hereafter labelled FeCo/Pt).
- $MgO/[Fe_{16.8\ Å}/Co_{12.2Å}]_{147}/Fe_{435Å}/V_{40Å}$ (hereafter labelled Fe/Co).

The experiments were carried out on the D17 neutron reflectometer at the Institut Laue Langevin, Grenoble, France [10]. The instrument is capable of working in both a time-of-flight (TOF) mode and a monochromatic mode, and measurements were carried out in both modes. The samples were placed in a 7 T horizontal cryomagnet with the field direction aligned along the surface normal. The field direction, which defines the axis for the neutron spin, was therefore parallel to **Q** for specular scattering

The efficiency of the multidetector was calibrated by measuring the small angle scattering from a standard sample of water.

The TOF mode was used for measuring the scattering with unpolarized neutrons. This method covers an extended range of momentum transfers in one measurement. The sample was aligned at an angle $\theta_i = 0.9°$ to the incident beam. The intensity was recorded as a function of measured time-of-flight for the neutrons to cover the distance between the D17 double chopper system and its two-dimensional detector. The usable wavelength range was between $\lambda \sim 2$–20 Å, and the wavelength distribution of the incident intensity was calibrated by measuring the main beam under the same resolution conditions as the reflectivity. The choppers were phased such that the relative wavelength resolution was $\Delta\lambda/\lambda \sim 1\%$.

The instrument was configured in monochromatic mode for further measurements with neutron polarization analysis. The incident beam was polarized using a magnetically saturated Fe/Si multilayer monochromator with a wavelength of $\lambda = 5.512$ Å. The reflected beam polarization was analysed using a ^{3}He polarized gas filter [12]. This configuration is optimal for the measurement of off-specular scattering with polarization analysis, as the filter covers the full angular range of the large multidetector. The neutron spin states before and

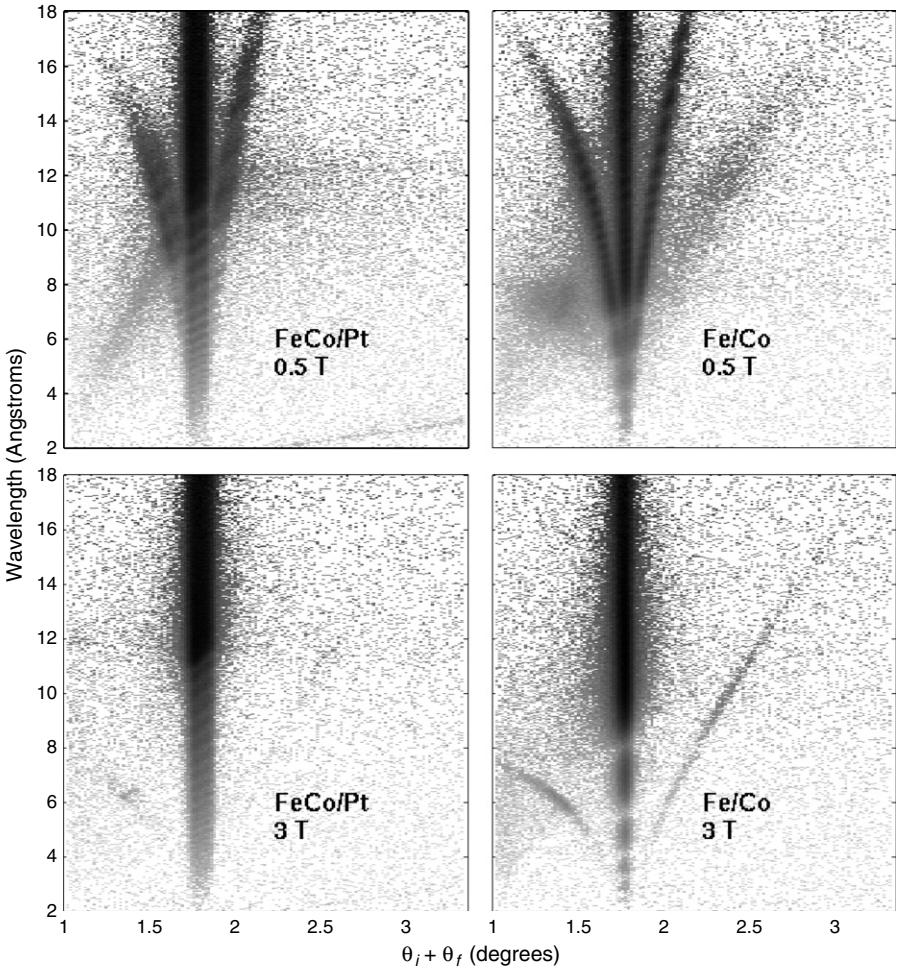

Figure 2. Field-dependent measurements of the specular and off-specular reflectivity of the FeCo/Pt and Fe/Co superlattices using unpolarized neutrons and time-of-flight mode. The incident angle, θ_i, was 0.9°. The data are plotted on a logarithmic scale. The features in the data are described in the text, and figure 3 shows their expected trajectories across the detector.

after the sample were chosen with the aid of spin flippers. Standard methods were used to calibrate the polarizing optics and to correct for inefficient polarization and for the time-dependence of the ^{3}He filter [11, 12]. In monochromatic mode, a series of measurements must be carried out to cover an acceptable range of momentum transfer. After alignment, the sample and detector were moved in a $(\theta, 2\theta)$ manner between measurements. This type of scan ensured that a single pixel on the detector satisfied the condition $\theta_i = \theta_f$ at all points.

3. Results

3.1. Unpolarized neutron reflectivity

Measurements of the samples in applied fields of 0.5 and 3 T are shown in figure 2. The data correspond to single scans in TOF mode and have been normalized to the incident beam intensity and corrected for detector efficiency. The wavelength, λ, is calculated from the time-of-flight that a neutron of constant speed would take to cross the distance between the choppers and the detectors. As previously discussed, spin flip scattering in a field results in a kinetic energy change in the neutron, hence the speed will not be constant. This change, however, results in a wavelength change that is at least an order of magnitude smaller than the resolution of the instrument, and therefore the calculated wavelengths are valid estimates.

When measuring in TOF mode, the scattering triangles observed in figure 1 appear as different trajectories across the detector. Figure 3 shows these trajectories, calculated for an arbitrary sample. There are three main features to be explained.

(i) Where $k_i = k_f$, specular reflectivity corresponds to $\theta_i = \theta_f$. In TOF mode, θ_i is fixed, the sum $\theta_i + \theta_f$ is constant, and thus this reflectivity appears as a vertical line on the detector.

(ii) Where $k_i \neq k_f$, equation (2) gives the relation between θ_i and θ_f when the momentum transfer of the reflected beam is normal to the surface. These trajectories are represented in figure 3 as a function of field and of whether the neutron has gained or lost kinetic energy on reflection.

(iii) In the presence of lateral correlations, scattering with a component of momentum transfer in the plane of the surface may be observed. Some of the brightest of these off-specular features will be observed for all $\theta_{i,f}$ where

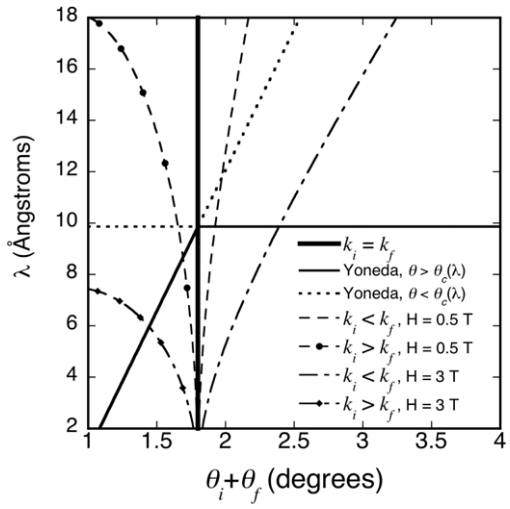

Figure 3. The calculated trajectories across the D17 detector for various features in neutron reflectivity as observed in a time-of-flight measurement.

$\theta_{f,i} = \theta_c(\lambda)$. This is known as Yoneda scattering [13]. The critical angle, $\theta_c(\lambda)$, is given by the equation:

$$\theta_c = \lambda\sqrt{N\bar{b}_{tot}/\pi}, \tag{3}$$

where N is the atomic number density and $\bar{b}_{tot}$ is a mean coherent scattering length density, including magnetization. Regarding figure 1, if $\theta_i = \theta_c$, Yoneda scattering could be expected for all the points that lie on the cut through the Ewald sphere. In TOF mode, the incident angle is fixed and the length of k_i changes. Hence the condition $\theta_i = \theta_c(\lambda)$ will hold for only one wavelength, and the Yoneda scattering will make a horizontal trajectory across the detector. From equation (3), the critical angle varies linearly with wavelength, hence the condition that $\theta_f = \theta_c$ corresponds to an oblique, straight line.

Inspection of figure 2 shows that features (i) and (ii) are clearly visible and follow the trajectories shown in figure 3. The trajectories of feature (ii) change with field in the manner expected from equation (2). In 0.5 T, both samples must therefore have components of the magnetization in the plane of the surface such that some neutron spins are flipped relative to the applied field. The Fe/Co sample shows some scattering of this nature even in 3 T, thus the sample retains some in-plane magnetization.

The Yoneda scattering is also clearly visible, but only in 0.5 T, indicating in-plane correlations. These correlations must therefore be purely magnetic, and the scattering would indicate the formation of domains with magnetizations that would have some component in-plane and some component out-of-plane. The absence of Yoneda scattering at the larger fields may be attributed to two effects: the realignment of the majority of the magnetization to point along the surface normal results in a concomitant decrease in magnetic scattering; and the in-plane domains either become significantly larger in 3 T, causing all the scattering to collapse to the specular trajectories, or very much smaller, such that the domain scattering becomes a weak, diffuse background.

There is, however, a remarkable difference in the Yoneda scattering between the FeCo/Pt and the Fe/Co samples. Yoneda scattering is normally observed only for $\theta_{i,f} > \theta_c(\lambda)$ when $\theta_{f,i} = \theta_c(\lambda)$. Comparison of figures 2 and 3 show that this is the case for the FeCo/Pt sample. On the other hand, the observed Yoneda for the Fe/Co sample shows that, for example, when $\theta_i = \theta_c(\lambda)$, the Yoneda scattering appears at $\theta_f < \theta_c(\lambda)$. This amounts to *sub-critical* Yoneda scattering, where significant off-specular scattering is seen *below* the critical edge.

Further information can be extracted by an appropriate integration over the detector, and these reflectivities are shown in figure 4.

The top two graphs show the total reflectivities of the samples in the two applied fields, integrated over the whole angular range of the detector. In a field of 3 T, both samples show total reflection at the longest wavelengths. In smaller fields the reflectivity is considerably changed for both samples, being significantly less than unity for longer wavelengths. That the longer wavelength reflectivity is less than unity may be understood if the off-specular scattering at the smaller field has a broader angular range than that covered by the detector and the integration is incomplete.

The $k_i = k_f$ reflectivities were extracted by integrating over the angle subtended by five detector pixels, centred on $\theta_i + \theta_f = 1.8°$. A similar procedure, centred on the appropriate pixel determined by equation (2), was used to extract the $k_i \neq k_f$ reflectivities. The data, extracted from the measurements made in 0.5 T, are shown in the bottom two graphs of figure 4. Both samples show oscillations in all the extracted reflectivities at the longest wavelengths, with the oscillations being more pronounced in the Fe/Co sample. Similar oscillations have been observed and explained by the coherent rotation of the neutron polarization on reflection [14, 15].

3.2. *Polarized neutron reflectivity*

To further characterize the sub-critical Yoneda scattering, the Fe/Co sample was re-measured with polarization analysis in an applied field of 0.5 T. Similar measurements have been done before on thin films of iron [16] and cobalt [17]. The resulting data, corrected for polarization inefficiency and time-dependence of the ^{3}He filter, are shown in figure 5. The data are plotted as a function of the flipper states, with the superscripts showing whether a flipper is off (0) or on (1). Features (i)–(iii), listed for the TOF data, are also observable in figure 5, although the trajectories differ in monochromatic mode. The trajectories are shown schematically in figure 6.

The polarizer and the analyser both transmit neutrons of the same spin state. Many of the features in figure 6 might be expected to appear for one of the flipper state combinations. The trajectory where $k_i = k_f$ corresponds to non-spin flip of the neutron and should therefore only be seen when both flippers are either on or off. The appearance of the two trajectories for $k_i \neq k_f$ would only be in the spin flip channels, i.e. when one of the flippers was on, and would depend on whether the

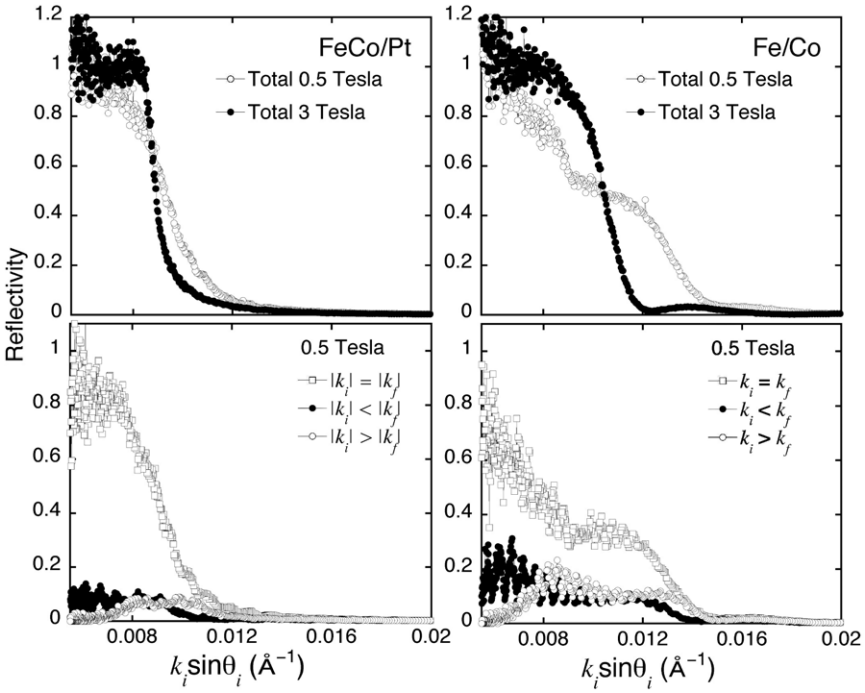

Figure 4. Reflectivity extracted from figure 2, plotted as a function of $k_i \sin\theta_i$, where $k_i = 2\pi/\lambda$. The plotted data correspond to a wavelength range of $4 \leqslant \lambda \leqslant 18$ Å. The top two graphs show the intensity integrated over $\theta_i + \theta_f$ on the detector, for the two samples in the two applied fields. The bottom two graphs show the intensities in an applied field of 0.5 T along the trajectories described in figure 3. They were calculated by integrating the detector over five pixels centred at the appropriate wavelength-dependent value of $\theta_i + \theta_f$.

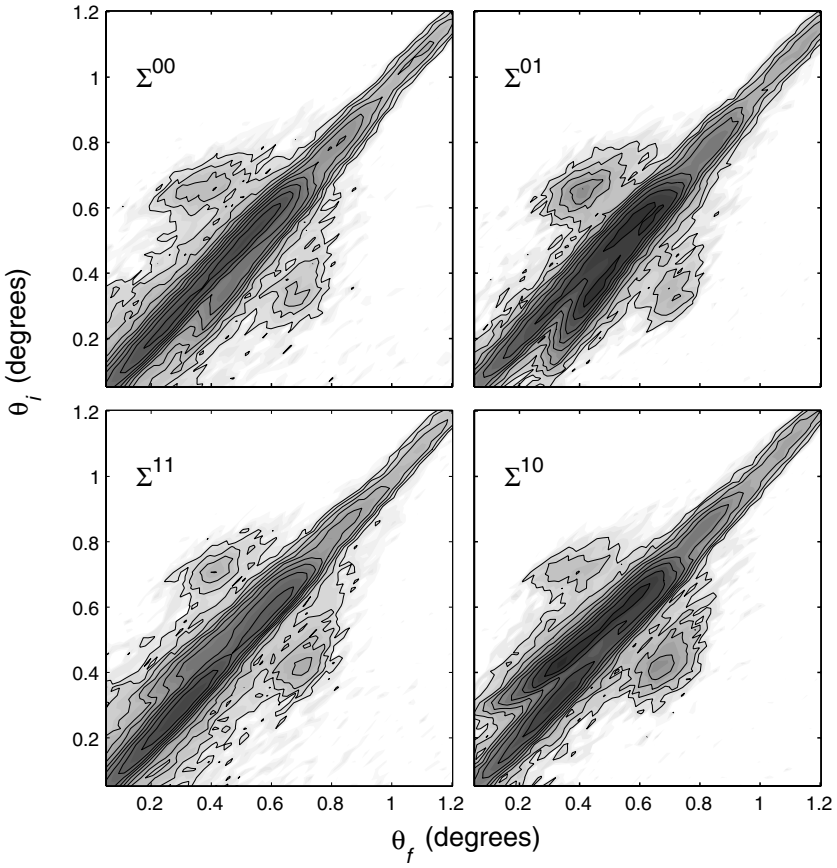

Figure 5. The polarization-dependent count rates, $\Sigma^{\alpha\beta}$, of the scattering from the Fe/Co sample, measured in an applied field of 0.5 T. The wavelength for the measurement was $\lambda = 5.512$ Å. The variables α and β refer to the flipper before and after the sample respectively. A value of α, $\beta = 0$ means that the flipper is off, while α, $\beta = 1$ means that the flipper is on. The data are plotted on a logarithmic scale.

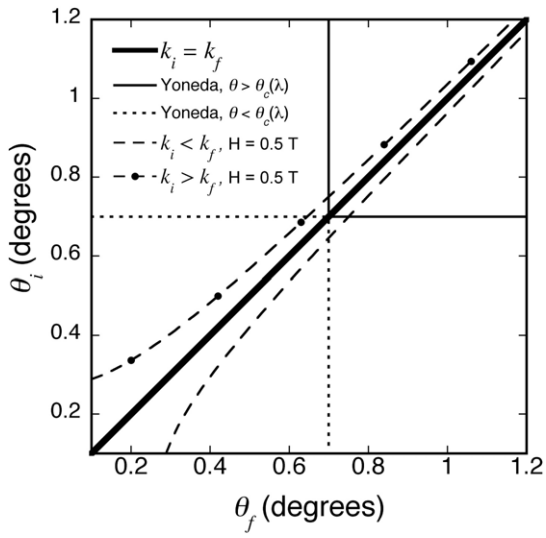

Figure 6. The calculated trajectories for various features in the reflectivity for a monochromatic scan on D17.

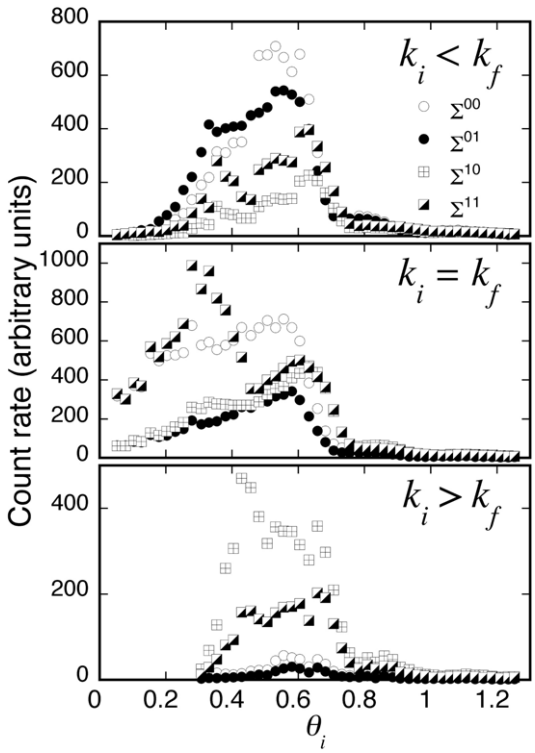

Figure 7. The count rates along the three trajectories given by $\theta_i = \theta_f$ and equation (2) from the data in figure 5. The data were calculated by integrating the intensity over five pixels centred at the appropriate θ_f.

initial neutron spin is parallel or antiparallel to the applied field. Yoneda scattering may be observed in all four channels, depending on the orientation of the magnetization with respect to the beam polarization.

Inspection of figure 5 shows that some of these trajectories appear in more than one channel. The $k_i = k_f$ trajectory is observed in all four channels. Each channel has one of the $k_i \neq k_f$ trajectories, with the particular trajectory depending on the first flipper state.

These observations are not a result of poor correction for imperfect instrumental polarization. The instrument was carefully characterized periodically during the measurement by translating the sample just out of the beam and measuring the flipping ratios of the main beam [12], and the resulting corrections properly accounted for the instrumental inefficiency. Furthermore, poor instrument polarization is quantitatively inconsistent with the data. The count rates along the different trajectories are shown in figure 7. Polarization corrections are derived from the valid assumption that the measured scattering is a linear combination of the proper polarization-dependent count rates [11], with coefficients that depend on the efficiency of the instrument. For this measurement, the coefficients do not change between data points, and any polarization 'leakage' would be angle independent. The data in figure 7, with very different angle-dependent behaviour, cannot be reproduced from polarization corrections. Thus, the data represent the real polarization-dependent intensities of the reflected beam.

4. Discussion

While the reflectivities from the FeCo/Pt superlattice appear to follow expected trends, the measurements of the Fe/Co superlattice have revealed effects that require more explanation. There are two observations that require particular attention: the observation of strong sub-critical Yoneda scattering, which is clearly linked to the magnetic structure of the sample; and the presence of spin-dependent reflectivity in unexpected polarization channels.

Further discussion requires a mathematical treatment of the polarized neutron reflectivity. A full polarization-dependent theory of grazing incidence neutron scattering, including off-specular scattering, is complex and arguably still in development. Many of the essential elements of the observed scattering, however, can be determined within the framework of the supermatrix method [18], which is a quantitative, dynamical scattering theory for specular reflectivity which considers the effects of the neutron polarization. The theory takes the characteristic matrix method developed for the treatment of electromagnetic waves in a stratified medium [19] and extends it to treat the neutron polarization using the theory of density matrices [20]. The method has no approximation for including roughness, nor of accounting for a reduction of intensity in specular reflection due to off-specular scattering. It also does not allow for splitting of the scattered beam due to a change in the neutron kinetic energy.

It does, however, calculate reflection, $\hat{R}$ and transmission $\hat{T}$ coefficients for arbitrary incident and final beam polarizations. These are sufficient to explain some of the observed off-specular events, hence this exact and easily programmable theory can be used to transparently build up a semi-quantitative picture of the off-specular scattering.

The coefficients $\hat{R}$ and $\hat{T}$ are (2×2) matrices within the supermatrix method. From these, the polarization-dependent reflectivity, $\mathcal{R}$, and transmission, $\mathcal{T}$, can be calculated from the

equations [15, 18]:

$$\mathcal{R} = \mathrm{Tr}\{\hat{\rho}_\mathrm{f}\hat{R}\hat{\rho}_\mathrm{i}\hat{R}^\dagger\}$$
$$\mathcal{T} = \frac{p_\mathrm{s}}{p_\mathrm{i}}\mathrm{Tr}\{\hat{\rho}_\mathrm{i}\hat{T}^\dagger\hat{\rho}_\mathrm{f}\hat{T}\}, \quad (4)$$

where $\hat{\rho}_{\mathrm{i,f}}$ are the spin-density matrices for the initial and final neutron states, $p_\mathrm{i} = k_\mathrm{i}\sin\theta_\mathrm{i}$, $p_\mathrm{s}^2 = p_\mathrm{i}^2 - 4\pi N_\mathrm{MgO}\bar{b}_\mathrm{MgO}$ and the superscript † refers to the Hermitian matrix.

A complete treatment of the full superlattice structures is the subject of another paper [9], however explanations for the two effects can be qualitatively shown by treating far simpler models for the two samples.

- The FeCo/Pt superlattice will be simplified to a three layer system on an MgO substrate (MgO/5.7 Å Fe/39 Å Pt/2400 Å $Fe_{0.175}Co_{0.311}Pt_{0.514}$). Following estimations from x-ray magnetic dichroism data [5, 6], the mean magnetic moment per atom of the FeCoPt alloy is taken to be 1.2 μ_B.
- The Fe/Co superlattice will be simplified to a two layer system on an MgO substrate (MgO/4738 Å $Fe_{0.58}Co_{0.42}$/435 Å Fe). The mean magnetic moment in the iron layer is taken as 2.2 μ_B/atom, while for FeCo alloy it is 2.08 μ_B/atom [7].

While obviously invalid for reflection at larger momentum transfers, this model holds roughly for reflection around and below the critical edge. Indeed, adopting more complicated models, including the full superlattice structure, gave much the same result. For the purposes of clarity it was decided to present the simulations from the simpler models.

Calculations of $\mathcal{R}$ for the two simplified models are shown in figure 8 for an incident angle of $\theta_\mathrm{i} = 0.9°$. The magnetic calculations assume that the entire moment per atom is lying in the plane of the film, i.e. no allowance has been made for the amount of the moment normal to the surface. This is largely valid in 0.5 T, as the out-of-plane direction is very hard for these samples, hence at this field the majority of the moments will still lie in the sample plane. Also shown is a calculation for a sample with no magnetization, which is identical to assuming that all the magnetization points along the surface normal and corresponds to the measurements made in 3 T. The nuclear and magnetic scattering lengths for the layers in the two models are shown in table 1. The initial and final neutron polarizations are collinear with the surface normal, i.e. the polarization is parallel to the scattering vector, as this is the direction of the applied field on the sample. The polarization-dependent simulations show that the non-spin flip reflectivities are equivalent, as are the spin flip reflectivities, hence only two of the four reflectivities are plotted.

The simulations for the reflectivity may be compared with the data in figure 4. The total reflectivities correspond relatively well, with the critical edges and overall wavelength dependence being reproduced in the simulations. The absence in the experimental data of the small oscillations observed in the simulations may be explained by the simplicity of the model used, which also did not include interfacial roughness.

The $k_\mathrm{i} = k_\mathrm{f}$ data in figure 4 may be associated with the non-spin flip simulations, and the $k_\mathrm{i} \neq k_\mathrm{f}$ with the spin flip. The simulations show oscillations in the polarization-dependent reflectivity that have similar periodicity to those observed in the experimental data. There are, however, significant differences. The magnitudes of the oscillations differ greatly, with the data showing small variations while the simulations oscillate between reflectivities of zero and one. The simulations also show that the two spin flip reflectivities are equivalent, while the data show not only differences in amplitude, but different apparent critical edges for $k_\mathrm{i} > k_\mathrm{f}$ and $k_\mathrm{i} < k_\mathrm{f}$. Some of the discrepancy in the amplitudes may be explained by three effects: the samples having less in-plane magnetization than the simulations as some will be pointing along the applied field direction; the limitations in the simplicity of the model and the application of the supermatrix method to measurements in a field; and some intensity in the specular reflection being lost to the strong off-specular scattering from the magnetic roughness. Nevertheless, the simulations will suffice for further explanation.

4.1. The source of sub-critical Yoneda scattering

Off-specular scattering can be considered with the distorted Born-wave approximation, which calculates the cross-section from a modified Fourier transform of the in-plane correlation function multiplied by the product of the squared transmission coefficients, $|T(\mathbf{k}_\mathrm{i})|^2|T(\mathbf{k}_\mathrm{f})|^2$ [21]. Within the supermatrix method, the squared transmission coefficients may be written $\mathrm{Tr}\{\hat{\rho}_\mathrm{i}\hat{T}^\dagger\hat{\rho}_\mathrm{f}\hat{T}\}$. Figure 8 also shows these quantities for the simplified models of the two superlattices. The coefficients are very different between the samples. For each sample, the values for non-spin flip are equivalent, as are the values for spin flip.

As previously discussed, the Yoneda scattering comes from magnetic correlations and therefore, with this scattering and polarization geometry, will be modulated by the relevant spin flip coefficients. The spin flip transmission coefficient for the FeCo/Pt sample has a peak at the critical edge. This is similar to that of reflection from a non-magnetic surface, where the squared transmission coefficients $|T(\mathbf{k}_{\mathrm{i,f}})|^2$ peak at a critical $k_{\mathrm{i,f}}\sin\theta_\mathrm{i} = \sqrt{4\pi\bar{b}_\mathrm{tot}}$ [19, 21]. Referring to figure 1, when $k_\mathrm{i}\sin\theta_\mathrm{i}$ is at this critical value the off-specular scattering along the whole trajectory swept out by $\mathbf{k}_\mathrm{f}$ would be multiplied by ∼5. The magnitude of the transmission coefficients is identical for $k_\mathrm{f}\sin\theta_\mathrm{i}$, which falls rapidly to zero below the critical edge and decreases slowly above it. The product of the two squared transmission coefficients results in a strong enhancement in the off-specular scattering for $\theta_\mathrm{f} > \theta_\mathrm{c}$ at the critical $k_\mathrm{i}\sin\theta_\mathrm{i}$, which corresponds to the observed Yoneda scattering.

In the Fe/Co sample, the spin flip transmission coefficients show a series of maxima *below* the critical $k_\mathrm{i}\sin\theta_\mathrm{i}$. The product of the squared transmission coefficients will therefore result in strong enhancements in the Yoneda scattering for $\theta < \theta_\mathrm{c}(\lambda)$, as was observed from this sample. This is a semi-quantitative explanation for the appearance of the sub-critical Yoneda.

The transmission coefficients alone clearly do not explain the observed scattering. The Yoneda scattering for the Fe/Co

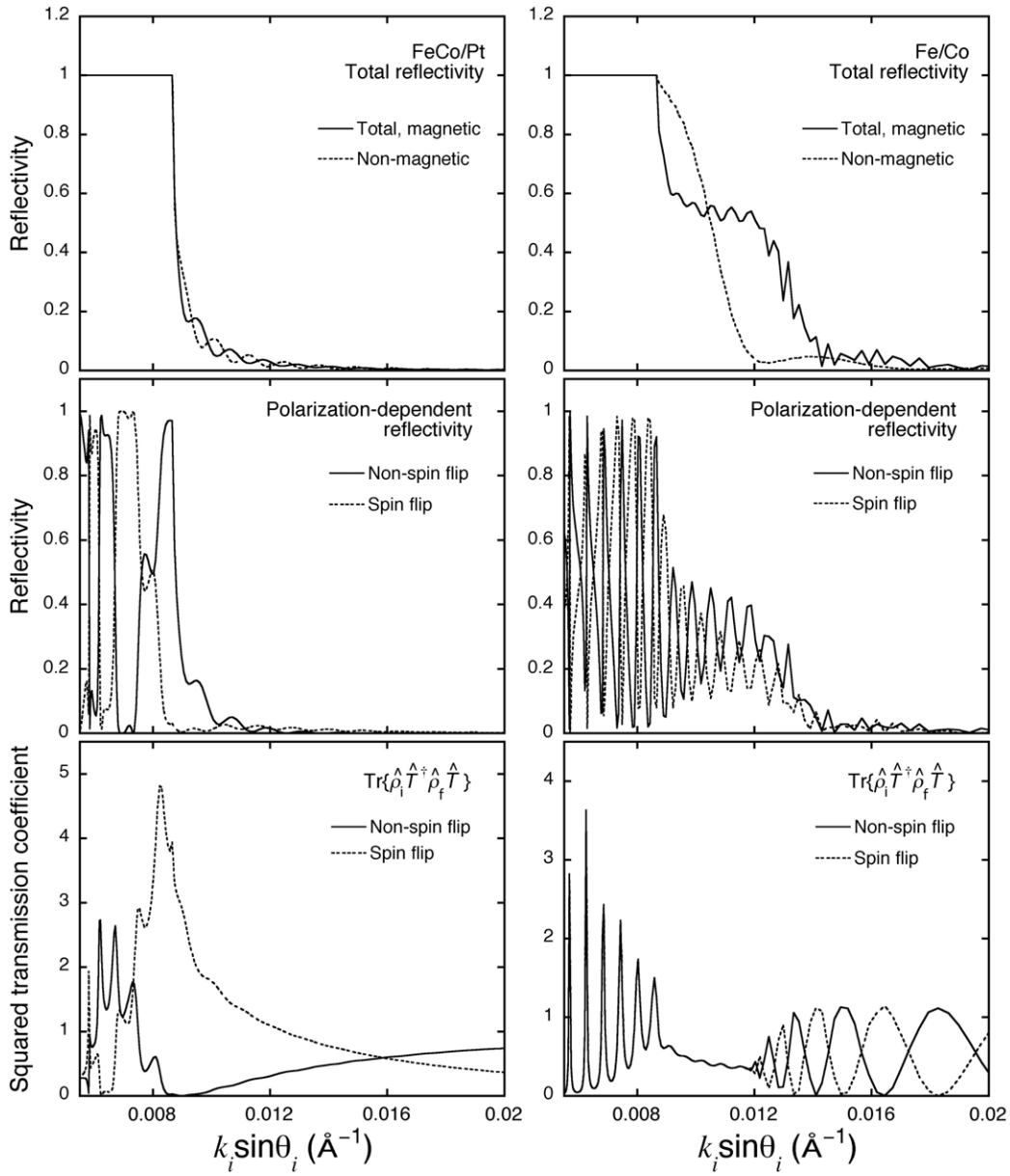

Figure 8. Simulations showing the reflectivity, $\mathcal{R}$, and squared transmission coefficients for simplified models of the two superlattices, as calculated using the supermatrix method [18] and an incident angle of $\theta_i = 0.9°$. The initial and final neutron polarization directions are along the surface normal. Also shown in the top two figures are the reflectivities for non-magnetic samples, calculated using the characteristic matrix method [19].

Table 1. Neutron optical quantities of the various layers for the two simplified models. Shown are the nuclear, b and magnetic, $(m_n\mu_n/2\pi\hbar)S\mu_B = CS\mu_B$, scattering lengths, and the associated scattering length densities p_N and p_M. The non-zero magnetic scattering lengths are calculated assuming that the whole moment per atom is lying in the plane.

FeCo/Pt					
Layer	Thickness (Å)	p_N (Å^{-2})	p_M (Å^{-2})	b (fm)	$CS\mu_B$ (fm)
$Fe_{0.175}Co_{0.311}Pt_{0.514}$	2400	2.263×10^{-5}	0.976×10^{-5}	7.363	2.174
Pt	39	7.855×10^{-5}	0	9.6	0
Fe	5.7	9.969×10^{-5}	6.139×10^{-5}	9.45	5.819
MgO	∞	7.515×10^{-5}	0	11.178	0
Fe/Co					
Fe	435	9.969×10^{-5}	6.139×10^{-5}	9.45	5.819
$Fe_{0.58}Co_{0.42}$	4738	7.11×10^{-5}	6.015×10^{-5}	6.502	5.501
MgO	∞	7.515×10^{-5}	0	11.178	0

sample shows only one, quite broad maximum, while the simulations would suggest that a number of maxima with widths that increase with increasing $k \sin\theta$ should be observed. This may be partly explained by the simplicity of the model, which did not allow for effects such as roughness that would broaden the widths and modulate the magnitudes of the maxima.

Furthermore, the squared transmission coefficients for the Fe/Co sample remain finite above the critical $k_i \sin\theta_i$, oscillating between zero and unity, although no Yoneda scattering is observed in the experiment. Within the distorted Born-wave approximation, the squared transmission coefficients need to be multiplied with a modified Fourier transform of the in-plane correlation function [21]. This function contains the in-plane magnetic and nuclear structure, including interfacial roughness, magnetic domain formation, and possible 'wandering axis' magnetic structures. The Fourier transform contains components of the neutron momentum transfer that are both in-plane, Q_x, and normal to the surface Q_z. The absence of the Yoneda scattering for $\theta_{i,f} > \theta_c$ could therefore be explained if this Fourier transform falls quickly with Q_z, hence the finite coefficients would be multiplied by a very small number given by the Fourier transform.

The reasons behind the unusual values of the transmission coefficients for the Fe/Co sample may be traced to its structure. The refractive index of a layer is given by the sum or difference, depending on the neutron spin orientation, of the nuclear and magnetic scattering lengths. Inspection of table 1 shows that these values are almost equivalent in the $Fe_{0.58}Co_{0.42}$ layer, while they are significantly different in the neighbouring layers. In particular, the scattering lengths for the Fe overlayer are larger than those for $Fe_{0.58}Co_{0.42}$. For one neutron spin state, the Fe/Co sample therefore has a potential well, with the possibility of neutron standing waves whose resonances will be given by the thickness of the layers [22–24]. The strong enhancements in the transmission coefficients of the Fe/Co sample below the critical edge may therefore be understood as neutron resonance states. The off-specular scattering in such cases might be expected to fall quickly with Q_z [22], consistent with the hypothesis above. Similar off-specular scattering has been seen in other samples that were said to have neutron resonance states [24] although the effect is far stronger in this sample.

The same conditions do not hold for the FeCo/Pt sample, which is more like a single magnetic layer on a non-magnetic substrate. Were this sample to have some nuclear roughness, enhancement of the non-spin flip Yoneda scattering might be expected below the critical edge.

4.2. The polarization-dependence of the reflectivity

Simple energy arguments show that the splitting of the specular beam is due to spin flip reflectivity, with a clear separation in reflected beams between spin flip and non-spin flip neutrons. Similar measurements on structurally simpler thin films of iron and cobalt have shown as much [16, 17], and have lead to suggestions that the splitting of the reflected beams might be exploited to do away with the need for an analyser. The measurements with polarization analysis, however, indicate that the reflected beams from the Fe/Co sample do not have unique neutron spin states.

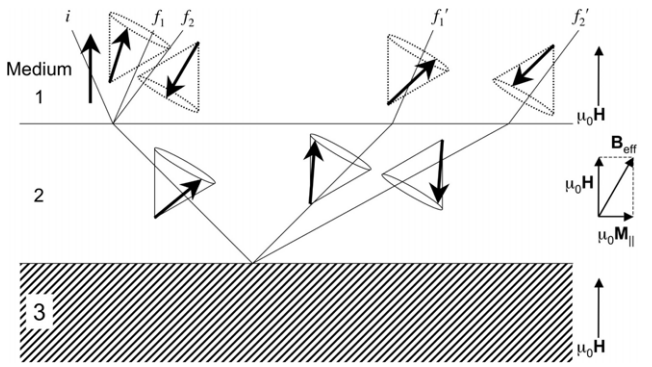

Figure 9. Schematic showing the rotation of the neutron polarization on reflection, and on passing through magnetic media. The magnetic fields in each medium are shown on the right hand side of the figure. Only medium 2 has an in-plane magnetization.

This apparent contradiction can be resolved if a distinction is made the neutron polarization axis and the axis along which the polarization is analysed. As pointed out by Pleshanov [25, 26], the quantization axis of a neutron beam does not have to be parallel to a given field direction. Pleshanov further states that it is impossible to make a single measurement that would correspond to a unique eigenstate of the neutron [25]. It is possible, however, to compare the measured intensities (as a function of the instrument flipper states) with the probability of the spin projection on to the field direction. Experimentally, this means that the projection of the polarization axis on to the analyser axis is measured.

A schematic representation of how the interaction can be classically visualized is shown in figure 9. The direction of the external magnetic field represents the direction of the initial polarization, and also the axis for the analyser. On interacting with the sample, which has components of magnetization that are perpendicular to the applied field, the polarization is rotated in a coherent manner about the axis $\mathbf{B}_{eff}$, represented in figure 9 by cones. The rotation will occur on passing through a magnetized layer as Larmor precession, and also on reflection from interfaces between layers with different magnetizations. It is this coherent rotation that has previously been described in numerous articles on the theory of polarized neutron reflectometry [3, 14–16, 18, 27, 28].

The splitting in the reflected beams results from a flip of the projection of the neutron polarization on to the axis of $\mathbf{B}_{eff}$. The value of $\mu_0 H$ associated with the change in the kinetic energy is the field strength applied on the sample. The cryomagnet used for the experiment has stray fields that fall rapidly with increasing distance from the sample. The kinetic energy change of the neutrons, giving rise to the split beams, must therefore occur at the point of reflection from the sample and nowhere else along the beam path. Spin flip scattering from the intrinsic magnetic field of the sample, established by its magnetization, must make no change in the kinetic energy. For example, iron has a saturation magnetization of $\sim 1.7 \times 10^6$ A m^{-1}, giving an average internal field of $\sim$2.1 T.

Neutron reflectivity from a thin magnetized film in a negligible applied field, however, results in the appearance of only one reflected beam corresponding to $k_i = k_f$. Equation (2) makes reference only to the externally applied field, $\mu_0 H$, and it is only due to this external field that the appearance of split beams may be observed.

In the schematic, two pairs of reflected beams are apparent. The beams f_1 and f_1' have had no change in the projection of their polarization and hence no change in their kinetic energy, while f_2 and f_2' correspond to the flipped projection. These pairs of reflected beams interfere in both their phase and their polarization, giving rise to the observed polarization-dependent reflectivity.

The experiment measured the projection of the beam polarization on to an axis, in this case that of the external magnetic field. The split beams have their own polarization dependences with respect to the magnetization of the sample. Although a change in kinetic energy is associated with flipping the *projection* of the polarization with respect to an external field, the final polarization of each beam *might not* be collinear with the initial polarization. The projection of the polarization of each beam on to the applied field axis will therefore show up as a *depolarization*, giving neutrons with spins both parallel and antiparallel to the analyser.

This type of behaviour was not observed in previous experiments [16, 17], however the samples measured were greatly different to the Fe/Co sample. In particular, the potential well-like structure of the Fe/Co sample may cause a significant enhancement of the rotation of the polarization.

A full, quantitative description requires a dynamical quantum theory of scattering to describe the propagation of the neutron wavefunction, including its spin, at every point in the sample. A number of these have been published for reflectivity (e.g. [3, 18, 27, 28]), however the majority give the result with respect to the initial and final neutron spin state defined by its quantization axis. For example, if the initial neutron spin state of a beam is defined as (+), the theories can be used to calculate the non-spin flip (++) and spin flip (+−) reflectivities. The implicit assumption is that the analyser axis is parallel to the quantization axis of the neutron. The scattered neutrons are interpreted as spin flip or non-spin flip according to the configuration of the flippers on the instrument.

This assumption is good if there is no splitting of the beams, as the evolution of the polarization at each point along the beam is correctly described, and the theories have been successfully used to model a wide range of polarized neutron reflectivity experiments. As they stand, however, these equations do not allow for an apparent depolarization of two split reflected beams. This may be irrelevant for many magnetic samples in an applied field, which can be modelled using the equations of Fermon [3]. For these, as an example, only one beam would be observed in a measurement with both flippers off, and this would correspond to the (++) reflectivity. The profile of the Fe/Co sample, with its deep potential well for one neutron spin state, may represent an unusual case where the assumption is not valid. While the supermatrix method currently does not account for the Zeeman-split beams, the rapid fluctuations between spin flip and non-spin flip in $\mathcal{R}$, shown in figure 8, attest to such a depolarization.

The supermatrix method has an advantage that the reflectivity can be solved for arbitrary incident and final polarization directions, including crossed polarizations. From this, a rotation matrix for the polarization can be derived [15] as can the polarization projection on to any given axis at the analyser [29]. Unfortunately, the method does not account for the splitting of the beam in an externally applied field and for the evolution of the polarization in the separate scattered beams. Extending the theory to allow for this is a priority, to be compared with data obtained from future experiments on specially tailored and fabricated samples.

5. Conclusions

The observations presented in this paper demonstrate some of the successes and some of the deficiencies of the theory describing neutron reflectometry. The supermatrix theory [18], for example, describes well the expected reflectivity in a negligible applied field. Applying this method to the data qualitatively explains many of the observed features, including oscillations in the reflectivity and sub-critical Yoneda scattering. The method fails, however, to adequately describe measurements in a reasonable field. The wave equation has been solved for polarized neutrons in an applied field and a corresponding matrix method has been developed [3]. Interpreting the data using these equations is difficult, however, as the axis of the final polarization of the split beams is not necessarily collinear with the axis of the applied field. The result is that scattering which is uniquely (non-)spin flip will be measured in apparently non-corresponding polarization channels.

Acknowledgments

Financial support from the Swedish Research Council (VR) is gratefully accepted. ARW would like to thank Dr R Cubitt for his critical reading of the manuscript.

References

[1] Zabel H, Theis-Bröhl K and Toperverg B 2007 *Handbook of Magnetism and Advanced Magnetic Materials* vol 3, ed H Kronmüller and S Parkin (New York: Wiley)
[2] Squires G L 1978 *Introduction to the Theory of Thermal Neutron Scattering* (Mieola: Dover)
[3] Fermon C 1995 *Physica* B **213/214** 910
[4] Felcher G P, Adenwalla S, de Haan V O and van Well A A 1995 *Nature* **377** 409
[5] Björck M 2007 *PhD Thesis*
[6] Björck M, Hedlund M and Andersson G 2008 *J. Magn. Magn. Mater.* at press
[7] Björck M, Andersson G, Lindgren B, Wäppling R, Stanciu V and Nordblad N 2004 *J. Magn. Magn. Mater.* **284** 273
[8] Andersson G, Björck M, Lidbaum H, Samyal B, Chacon C, Zlotea C and Valizadeh S 2007 *J. Phys.: Condens. Matter* **19** 016008
[9] Björck M, Andersson G, Sanyal B, Hedlund M and Wildes A 2008 *Phys. Rev.* B submitted
[10] Cubitt R and Fragneto G 2002 *Appl. Phys.* A **74** S329
[11] Wildes A R 2006 *Neutron News* **17** 17

[12] Andersen K H, Cubitt R, Humblot H, Jullien D, Petoukhov A, Tasset F, Schanzer C, Shah V R and Wildes A R 2006 *Physica* B **385/386** 1134
[13] Yoneda Y 1963 *Phys. Rev.* **131** 2010
[14] te Velthuis S G E, Felcher G P, Blomquist P and Wäppling R 2001 *J. Phys.: Condens. Matter* **13** 5577
[15] Toperverg B P, Lauter H J and Lauter-Pasyuk V V 2005 *Physica* B **356** 1
[16] van de Kruijs R W E, Fredrikze H, Rekveldt M T, van Well A A, Nikitenko Y V and Syromyanikov V G 2000 *Physica* B **283** 189
[17] Hussey D, Fan S, Neff B, Bailey C, Snow W M, Rich D, Thompson A K, Gentle T R, te Velthuis S G E and Felcher G P 2002 *Appl. Phys.* A **74** S234
[18] Rühm A, Toperverg B P and Dosch H 1999 *Phys. Rev.* B **60** 16073
[19] Born M and Wolff E 1999 *Principles of Optics* (Cambridge: Cambridge University Press)
[20] Blume M 1963 *Phys. Rev.* **130** 1670
[21] Sinha S K, Sirota E B, Garoff S and Stanley H B 1988 *Phys. Rev.* B **38** 2297
[22] Pfeiffer F, Leiner V, Høghøj P and Anderson I 2002 *Phys. Rev. Lett.* **88** 055507
[23] Aksenov V L, Ignatovich V K and Nikitenko Y V 2006 *Cryst. Rep.* **51** 734
[24] Kentzinger E, Rücker U, Toperverg B and Brückel T 2003 *Physica* B **335** 89
[25] Pleshanov N K 1999 *Phys. Lett.* A **259** 29
[26] Pleshanov N K 2001 *Physica* B **304** 193
[27] Blundell S J and Bland J A C 1992 *Phys. Rev.* B **46** 3391
[28] Radu F and Ignatovich V K 1999 *Physica* B **267/268** 175
[29] Toperverg B P 2001 *Physica* B **297** 160